Received: 29 November 2018 | Revised: 20 August 2019 | Accepted: 22 October 2019

DOI: 10.1002/ppp.2036

RESEARCH ARTICLE

WILEY

Unmanned aerial vehicle-based mapping of turf-banked solifluction lobe movement and its relation to material, geomorphometric, thermal and vegetation properties

Jana Eichel[1] | Daniel Draebing[2,3] | Teja Kattenborn[1] | Johannes Antenor Senn[1,4] | Lasse Klingbeil[5] | Markus Wieland[5] | Erik Heinz[5]

[1]Institute of Geography and Geoecology, Karlsruhe Institute of Technology, Karlsruhe, Germany

[2]Chair of Geomorphology, University of Bayreuth, Bayreuth, Germany

[3]Chair of Landslide Research, Technical University of Munich, Munich, Germany

[4]School of Engineering, Newcastle University, Newcastle upon Tyne, UK

[5]Institute of Geodesy and Geoinformation, University of Bonn, Bonn, Germany

Correspondence
Jana Eichel, Institute of Geography and Geoecology, Karlsruhe Institute of Technology, Karlsruhe, Germany.
Email: jana.eichel@kit.edu

Funding information
Gesellschaft für Erdkunde zu Berlin, Grant/Award Number: Humbold-Ritter-Penck Stiftung; Gesellschaft für Erdkunde zu Köln e.V., Grant/Award Number: Dr. Hohmann award; German Research Foundation DFG, Grant/Award Number: DI 414/22-1

Abstract

Solifluction is one of the most widespread periglacial processes with low annual movement rates in the range of ¯millimeters to centimeters. Traditional methods to assess solifluction movement usually have low spatial resolution, which hampers our understanding of spatial movement patterns and the factors controlling them. In this study, we (a) test the applicability of unmanned aerial vehicle (UAV)-based structure-from-motion photogrammetry in comparison to a traditional total station survey to map surface movement of a turf-banked solifluction lobe (TBL) in the Turtmann Valley (Switzerland). We then (b) relate the detected movement patterns to potential geomorphometric, material, thermal and vegetation controls, which we assessed using geomorphic and vegetation mapping, electrical resistivity surveys and temperature loggers. Our results show that (a) UAV-based mapping can detect solifluction movement with high spatial resolution (one point per m^2, total > 900 points) and rates and patterns consistent with a total station survey, but requires careful measurement set-up and analysis; and (b) movement rates differ between lobe tread, riser and a ridge feature. Differences can be explained by heterogeneous material, geomorphometric, thermal and vegetation properties of the TBL, which promote different solifluction processes. Our study demonstrates the applicability of UAV-based mapping in solifluction research and improves our understanding of solifluction processes and landform development.

KEYWORDS

biogeomorphology, electrical resistivity tomography, periglacial processes, photogrammetry, solifluction, UAV

1 | INTRODUCTION

Solifluction is the slow downslope movement of soil mass due to needle-ice creep, frost creep, gelifluction and plug-like flow.[1] Solifluction movement rates are comparatively low, usually of the order of millimeters to centimeters per year. However, solifluction contributes substantially to sediment transport and total slope retreat due to its widespread distribution.[1-3] Solifluction can either continuously rework slope material in the form of solifluction sheets or produce more distinct solifluction landforms. Solifluction landforms include solifluction

terraces made up of steps or benches and isolated, tongue-shaped solifluction lobes, consisting of a lobe tread bordered by lateral and a frontal riser.[4] Landforms with fronts covered by vegetation are called turf-banked, whereas landforms with stony fronts are called stone-banked. Factors controlling solifluction movement include (a) material properties, such as soil texture and moisture, (b) topographic controls, such as slope angle, (c) climatic controls including air and soil temperatures and snow cover, and (d) the occurrence of permafrost.[1,5,6] Recent research has highlighted the role of vegetation in influencing solifluction processes and the development of solifluction landforms.[7,8] It was suggested that certain plant species, for example the arctic-alpine dwarf shrub *Dryas octopetala* L., influence mechanical, hydrological and thermal material properties through their characteristic functional traits, such as strong roots and dense mat growth. These ecosystem engineers thus change the geomorphic processes that occur by trapping frost-susceptible fines and could promote solifluction movement and the development of turf-banked solifluction lobes (TBLs).[8-10] In a mature solifluction lobe development stage, late-successional vegetation species replace engineering species and constrain solifluction movement.[8]

Traditionally, solifluction movement is measured both continuously at and below the surface at a single location or discontinuously at the surface using tape or point geodetic measurements of markers (e.g., total station surveys). Continuous measurements of solifluction movement are carried out using strain probes,[11] inclinometers[12] or potentiometers[13] installed at several depths to assess volumetric soil movement. These techniques have high temporal resolution and are usually combined with the assessment of potential controlling factors (e.g., soil moisture and temperature) at the same site. However, their explanatory power is limited to the point location and extrapolation to the landform scale is difficult to impossible due to spatial variation of controlling factors such as soil moisture.[4,7] Discontinuous measurements of surface velocity are carried out in regular intervals (e.g., each year) using either tape measures[12,14-16] or total station surveys.[4,11,13,17,18] These techniques measure the distance from a stable and fixed reference point or benchmark to markers, typically painted rocks, painted lines, or wooden or steel pegs. Discontinuous measurements can be very time-consuming and, therefore, generally have low spatial resolution with a maximum of some tens of points per solifluction lobe. In addition, measurement errors can be high, for example up to 1 cm for tape measurements due to a combination of operator and methodological errors.[16] Using time-lapse photography, the temporal resolution of the described techniques can be increased strongly.[19]

Previous research has shown that solifluction movement patterns can be highly heterogeneous in space.[1] This variation can cause the development of different solifluction landforms such as lobes, sheets and terraces.[14,15,20] Yet, landform development is still not completely understood as high-resolution data on solifluction movement in time and space is missing. To close this gap and link solifluction movement patterns to potential controls, it is necessary to assess solifluction movement with a higher spatiotemporal resolution than commonly delivered by traditional methods. On a landscape scale, space-based Interferometric Synthetic Aperture Radar (InSAR) was used to determine freeze–thaw activity and surface movement of solifluction sheets with a high spatiotemporal resolution.[21,22] At landform scales, unmanned aerial vehicle (UAV)-based or terrestrial structure-from-motion (SfM) photogrammetry have shown good results in detecting geomorphic changes with a high spatiotemporal resolution on hillslopes and in fluvial environments.[23-25] In periglacial geomorphology, SfM photogrammetry has recently been successfully used in a number of applications, including landform mapping,[26] monitoring of needle-ice formation and frost heave,[27] assessment of rock glacier movement[28-30] and determination of the surface kinematics of sorted circles.[31]

However, to our knowledge, UAV-based SfM photogrammetry has not yet been applied to determine solifluction movement rates and patterns in relation to environmental properties. As UAV-based mapping can provide movement rates with a high spatial resolution, this novel technique can help to understand the spatial heterogeneity of solifluction movement. In combination with detailed data on potential solifluction controls, it can also improve our understanding of solifluction landform dynamics and development. Consequently, our objectives here are:

1. To evaluate the applicability of UAV-based SfM photogrammetry to map solifluction movement at a TBL.
2. To quantify spatial patterns of solifluction lobe movement and link them to potential material, geomorphometric, thermal and vegetation controls.

2 | STUDY AREA

The investigated TBL is located between 2,170 and 2,185 m a.s.l. on a distal lateral moraine slope in the Turtmann glacier foreland, Switzerland (Figure 1a). The lateral moraine slope parenting the lobe was formed by a smaller glacier advance of the Turtmann Glacier in 1925. Moraine material consists of middle-penninic marbles from the Barrhorn series and paragneiss and schistose rocks from the Mischabel crystalline complex, as well as higher penninic calcareous shales and greenstones from the Tsaté nappe and austroalpine gneiss and gabbro from the Dent Blanche nappe.[32,33] Mean annual air temperatures derived from a climate station at 2,180 m a.s.l. in the glacier foreland ranged from 1.8 to 3.89°C between 2014 and 2017, and annual precipitation ranged from 720.4 to 835.4 mm.[34] The study area is located 250–300 m below the lower limit of permafrost derived from rock glacier distribution.[35] Consequently, permafrost is not influencing current solifluction processes. The TBL itself is 29 m long and up to 14 m wide (Figure 1b), with its tread inclined at 22° while the parent slope gradient is 23°.[7] Its frontal riser is up to 1.8 m high and consists of multiple steps, and lateral risers are up to 1 m high. Previous investigations have shown that the lobe tread material consists of sandy silt, while larger clasts often occur at the lobe risers.[7] The lobe tread is covered by the ecosystem engineer *D. octopetala* except for a sparsely vegetated longitudinal, ridge-like feature in the upper center of the tread.[8]

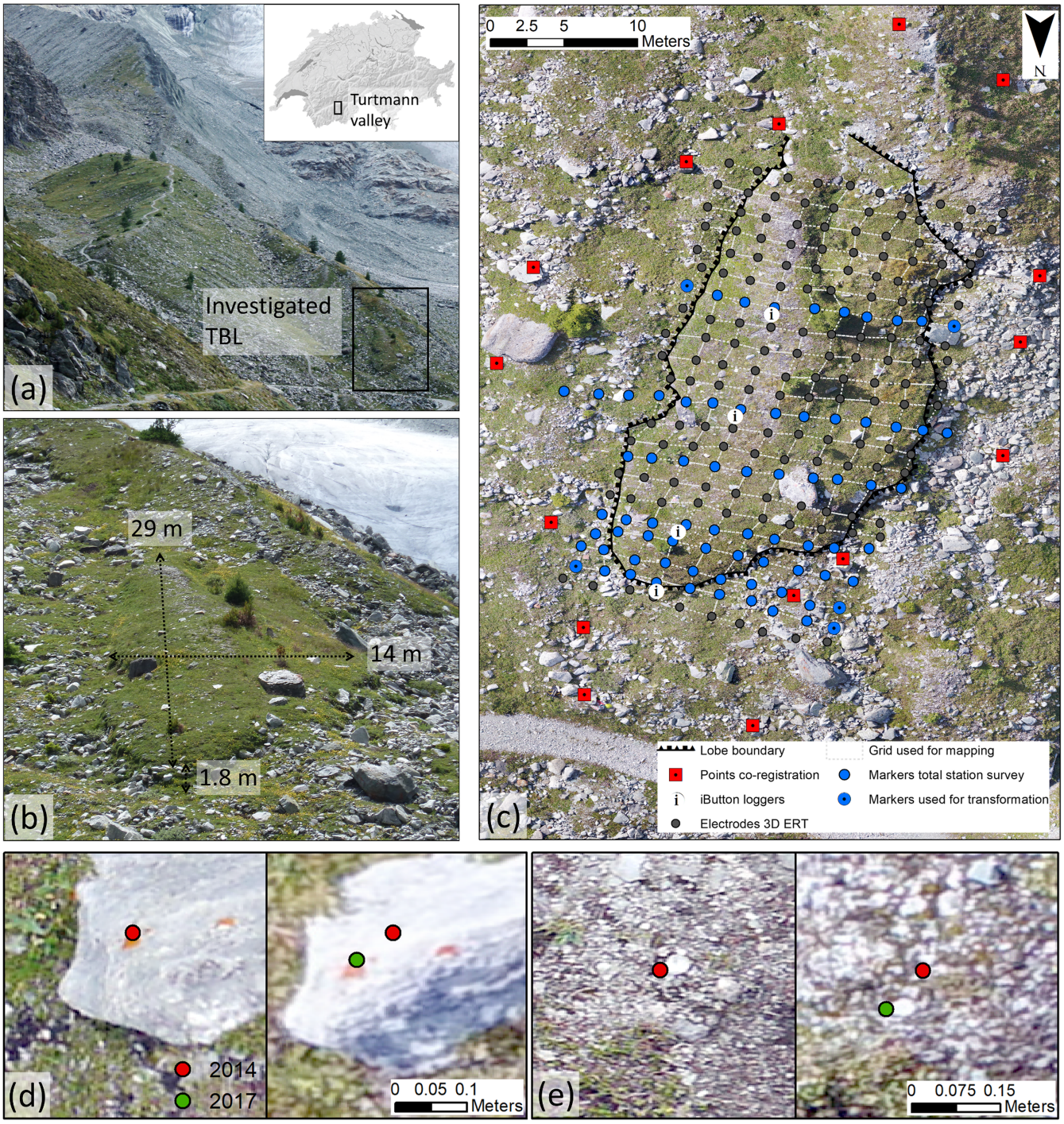

FIGURE 1 (a) Investigated turf-banked solifluction lobe (TBL) located at distal lateral moraine slope in Turtmann glacier foreland, Valais, Switzerland. (b) Close-up view of the investigated TBL with highlighted dimensions. (c) Measurement set-up at the TBL with electrode positions for 3D ERT, grid used for geomorphic and vegetation mapping, position of iButton temperature loggers, total station survey markers, also used as ERT electrodes, and reference points used for image co-registration. Total station markers used for transformation in a common coordinate system are shown. (d,e) Examples of tracked features: distinctive lichens on a larger boulder and a small cobble set firmly into the soil [Colour figure can be viewed at wileyonlinelibrary.com]

3 | METHODS

3.1 | UAV surveys, photogrammetric data processing and movement detection

To assess lobe movement, UAV surveys were carried out at the TBL on August 14, 2014 and August 17, 2017. The 2014 UAV survey was carried out using a customized Mikrokopter OktoXL Oktokopter (HiSystems GmbH, equipped with Panasonic Lumix GX1, of 16 Mpixel, and 22 mm fixed focal length) manually flown at a height of roughly 15 m. Derived aerial imagery (416 images) was processed in Agisoft Photoscan (Version 1.2.6). The corresponding SfM approach includes the detection of keypoints, which are used to estimate the camera

position of each image through a bundle adjustment.[24,25] The resulting sparse point cloud (corresponding keypoints) was georeferenced based on five ground control points (GCPs) measured using a differential GPS (Leica GPS1200 GNSS with RTK) with accuracies of about 2–3 cm. Using the triangulated images and the sparse point cloud, a densification process was then performed (Multi View Stereo, MVS) to generate the so-called dense point cloud. Based on the dense point cloud, a digital surface model (DSM) is produced on which the image textures are projected to produce an orthophoto. Here, the DSM and orthophoto produced in this way have a spatial resolution of 2 mm and an accuracy of 5 mm. The latter is a value for the internal accuracy, derived by building the mean length of the GCP residuals. The 2017 UAV campaign was carried out using a Phantom 4 Pro+ (20-Mpixel built-in camera, 24-mm fixed focal length), again flown manually at a height of 15–20 m. Based on 15 comparatively stable reference points (e.g., features on non-moving rocks) identified in the field (Figure 1c), the 2017 aerial imagery (total 564 images) was co-registered on the 2014 orthophoto. Coordinates for the stable reference points were extracted from the 2014 orthophoto and DSM. The co-registration was then carried out in Agisoft Photoscan (Version 1.4.0), where the stable reference points were used as ground control points to optimize image triangulation. Subsequently, the DSM and orthophoto with 2-mm resolution were derived.

On the orthophotos, manual feature tracking was carried out in ArcGIS with the help of a 1.5 × 1.5-m grid placed on the orthophoto and used for orientation. In previous geomorphic studies on glacier movement, manual feature tracking showed good results in comparison with automatic methods.[36] Criteria for the selection of tracked features included (a) high visibility and recognizability in both orthophotos as well as (b) discrete, distinct and easily identifiable feature borders. Examples of tracked features are small patches of lichen and moss on larger clasts (Figure 1d), as well as edges of pebbles, stones and rocks (Figure 1e). Dense vegetation cover strongly limited feature tracking and no discrete matching features could be identified in areas with high vegetation cover. If vegetation cover permitted tracking, at least one feature was tracked per grid cell in areas outside the lobe. On the lobe, the number of tracked features was increased to at least three per grid cell and to more than 10 per grid cell in areas with irregular displacement patterns such as the ridge feature and the risers. Thereby, small-scale movement differences could be evaluated. In total, we tracked 975 features in an area of 867 m^2 and calculated displacement based on the distance between the features in 2014 and 2017. Mean annual displacement rates were calculated for all tracked features at (a) the entire lobe, (b) different lobe areas (tread, ridge, risers) and (c) the adjacent parent slope area. Subsequently, we used a *t*-test to assess if the mean displacement values differed significantly between lobe and parent slope.

3.2 | Total station measurements

To validate UAV-derived solifluction movement rates and patterns, traditional total station measurements of solifluction movement were carried out for one season (2014–2015) at the lobe. Seventy steel pin markers were arranged in seven parallel rows crossing the lobe from west to east (1.5-m spacing between pins in row) and measured with a total station in 2014 and 2015 (Figure 1c). To improve measurement accuracy, small holes (~5 mm in diameter, 3 mm in depth) were drilled into the pin tops to place the reflector precisely. The estimated accuracy of the measured points was <1 cm. Five steel pin markers on the parent slope, which are assumed to be stable over time (Figure 1c), were used to transform the points from 2014 and 2015 into a common coordinate system. Following this, point displacements between the two measurements were calculated and tested for significance using a Fisher test. This was performed according to the classical strategy as used for geodetic monitoring applications, such as of landslides.[37] Potential error sources of this approach include movement of stable points used for coordinate system transformation and potential steel pin movement during ERT surveys.

3.3 | Assessment of material, geomorphometric, thermal and vegetation factors

To determine potential controls and indicators of lobe movement, we quantified material, thermal and vegetation properties at the TBL. At the same lobe investigated in this study, Draebing and Eichel developed a 3D Electrical Resistivity Tomography procedure which used 220 electrodes, including the 70 steel pin markers from the total station survey, in 22 parallel transects with an electrode spacing of 1.5 m in a roll-along manner[7] (Figure 1c). Their study showed that electrical resistivity fluctuates in the short term due to differences in soil moisture; however, spatial patterns of resistivity are constant and indicate differences in material properties. For this study, we repeated the measurement procedure on August 17, 2015 using an ABEM Terrameter LS device. For a detailed description of data acquisition and processing see the paper by Draebing and Eichel.[7]

The ERT grid was used as a reference for geomorphic and vegetation mapping. In each grid cell, we mapped surface material properties and lobe elements as well as where individuals of each plant species occurred (cf. Eichel et al.[8]). For *D. octopetala*, we additionally mapped its cover outlines in the grid cells. Subsequently, we created detailed geomorphic and vegetation maps (1:50) in ArcGIS, which show the species distribution in relation to the lobe elements (tread, risers, ridge). In the maps thus created, locations of individuals of a species are denoted by a symbol. Furthermore, a slope gradient map representing the main trends in slope gradient was derived from the 2014 DSM using a resampled version (resolution 0.25 m). A detailed description and discussion of geomorphic and vegetation properties of the studied TBL is given by Eichel et al.[8]

Soil temperatures of the lobe were measured between July 31, 2014 and August 24, 2016 in four positions along the central lobe axis (Figure 1C) using Maxim iButton miniature temperature loggers. The iAssist software[38] was used for logger programming and data read out, while data analysis was carried out in R (R Core Development Team). The temperature loggers recorded soil temperatures at

5 cm depth in 3-hr intervals with an accuracy of ±0.25°C. Temperature data accuracy was improved using the zero-curtain period as a 0°C reference.[8] The corrected temperature data were used to calculate mean annual ground surface temperature (MAGST), mean winter ground surface temperature (MWGST, December–February), mean summer ground surface temperature (MSGST, June–August) and the annual sum of daily sub-zero temperatures. Snow cover duration was derived using the standard deviation approach given by Schmid et al.[39] To provide a coarse estimate of potential diurnal solifluction movement contained in determined annual movement rates, the number of freeze–thaw cycles (FTCs) occurring, defined as temperature fluctuations with a temperature decrease below 0°C followed by an increase above 0°C, was determined.

4 | RESULTS

4.1 | Solifluction movement rates and patterns

Results from feature tracking in the orthophotos from 2014 and 2017 show that surface displacement rates in the considered area range between 0 and 16.5 cm over 3 years (0–5.5 cm yr^{-1}), with the TBL moving more quickly than its surrounding parent slope (Figure 2a). Registration accuracy for the two orthophotos is 0.8–4.8 cm, suggesting a possible error in the detected displacement rates of around 3.05 cm (average registration error). The *t*-test shows that mean displacement rates differ significantly ($p < 0.001$) between the TBL and parent slope. The mean displacement rate of the parent slope is 2.0 cm in 3 years (0.66 cm yr^{-1}), and displacement generally increases with distance to the lobe (Figure 2a). Highest displacement of the parent slope (>3–5 cm in 3 years) occurs west and southeast of the TBL, mostly in near turf-banked terraces (Figure 2a). The mean displacement rate of the TBL is 4.65 cm in 3 years (1.55 cm yr^{-1}). Displacements range from 0.27 to 16.29 cm in 3 years and result in distinct internal spatial displacement patterns (Figure 2a). The lobe tread moves more quickly, up to 16.5 cm in 3 years (mean 1.57 cm yr^{-1}), than the lobe risers (up to 8 cm in 3 years, mean 0.63 cm yr^{-1}). High displacement occurred in particular along the central lobe axis, often 5–8 cm in 3 years (mean 1.9 cm yr^{-1}), with highest displacement rates at the lower lobe tread (often >8–16.5 cm in 3 years, mean 1.96 cm yr^{-1}; Movie S1). Slightly lower displacement rates of generally 3–5 cm in 3 years (mean 1.2 cm yr^{-1}) characterize the ridge

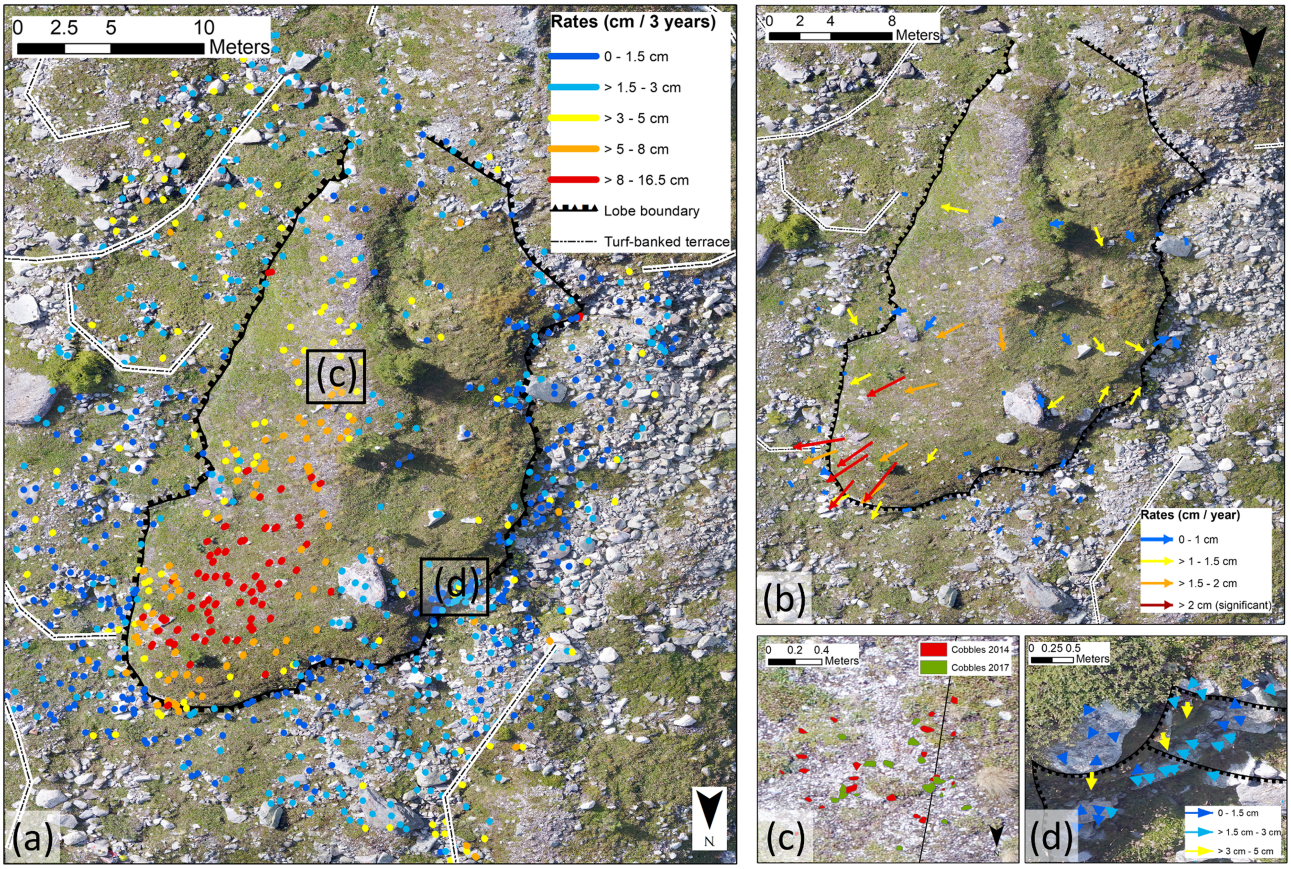

FIGURE 2 Results from unmanned aerial vehicle-based mapping and total station survey of solifluction movement. (a) Displacement rates (2014–2017) and spatial displacement patterns at the investigated turf-banked solifluction lobe and the adjacent parent slope. Further solifluction features (turf-banked terraces) are marked based on mapping by Eichel *et al.*[45] (b) Displacement rates derived from total station measurements in 2014 and 2015. (c) Close-up of displacement patterns of small cobbles at the lobe ridge. (d) Close-up of irregular displacement at the western lateral lobe riser [Colour figure can be viewed at wileyonlinelibrary.com]

feature at the upper central part of the lobe (Figures 2a, 3a). In contrast, lower displacement occurred at the western lobe tread (up to 3 cm in 3 years) and at the lateral risers (mostly up to 3 cm in 3 years, mean 0.54 cm yr^{-1}; Figures 2a, 3a), whereas the eastern frontal riser moved more quickly (>3 cm and up to 16.5 cm in 3 years, mean 1.26 cm yr^{-1}; Figure 2a).

In more detail, interesting small-scale displacement patterns appear at the ridge feature and the western lateral riser. At the ridge feature, an irregular displacement of small cobbles between 2014 and 2017 can be observed. Cobbles strongly changed their position and/or orientation during this period, which impedes feature tracking (Figure 2c). At the western lateral riser, analysis of small-scale displacement shows that rocks and boulders in the upper part of the riser are toppling downslope towards the parent slope, while boulders in the lower part are in contrast moving towards the lobe (Figure 2d).

Results from total station measurements show similar displacement patterns for the surveyed points between 2014 and 2015 (Figure 2b) with mean rates of 0.83 cm yr^{-1}. The largest and significant (> 2 cm yr^{-1}) displacements were detected at the eastern lower lobe tread, with mean rates of 2.18 cm yr^{-1}. A clear displacement trend pointing downslope is evident in most parts of the lobe, although non-significant upslope displacement was detected in some parts of the eastern lobe tread. Assumed stable markers show mean differences of 0.36 cm between 2014 and 2015. However, these differences have no trend and are within the expected accuracy of the total station measurements, so markers are treated as stable in the analysis.

4.2 | Material, geomorphometric, thermal and vegetation properties in relation to movement patterns

Movement patterns detected in the UAV-based mapping approach relate to material, geomorphometric, thermal and vegetation properties of the TBL. The geomorphic map (Figure 3a) shows that the area around the ridge with intermediate displacement rates (>3–8 cm in 3 years) is characterized by fine and coarse soil (<63 mm). In contrast, boulders (>200 mm) often occur in riser positions with low displacement rates (up to 3 cm in 3 years). The 3D ERT result (Figure 3c, d) shows that areas of low resistance (<0.71 kΩm) occur along the central lobe axis in the uppermost 0.75 m in the area with the highest displacement rates (>3–16.5 cm in 3 years; Figure 3c). High resistivities (>7.1 kΩm) characterize the lateral and frontal lobe risers at depths of 0–1.5 m in areas with lower displacement rates (0–5 cm in 3 years; Figure 3c, d). The slope gradient map (Figure 3b) shows that the slope gradient is slightly higher (15–35°) at the most quickly moving lower lobe tread (> 8–16.5 cm in 3 years) than at the more slowly moving ridge feature (slope gradient 0–25°).

Data from iButton temperature loggers show a decreasing trend in MAGST, MSGST, maximum temperatures and the annual sum of daily sub-zero temperatures along the central lobe axis from the ridge feature to the frontal riser, while MWGST values increase along the central axis (Figure 4, Table 1). These trends are mostly consistent from 2014/2015 to 2015/2016; only in 2015/16, the iButton logger at the lower tread (iB3) shows slightly higher MAGST than the iButton at the center of the tread (iB2). However, all GSTs are lower in 2015/2016 than in 2014/2015, which is especially highlighted in much lower MWGSTs (lowest MAGST in 2014/2015 −1.1°C, in 2015/2016 −4.41°C), and an increase of the annual sum of sub-zero temperatures (3.4- to 4.9-fold increase from 2014/2015 to 2015/2016). Snow cover duration is generally shorter in 2015/2016 than in 2014/2015 and shows an increasing trend of longer snow cover from the lobe ridge towards the frontal riser in both years, except for iB4 at the frontal riser in 2014/2015. In 2014/2015, the number of FTCs decreases along the central axis from the lobe ridge (11 FTCs, 10 of which diurnal) to the frontal riser (two FTCs, one diurnal). Freeze–thaw activity is generally higher in 2015/2016 (9–15 FTCs, 8–14 diurnal) compared to 2014/15. Annual FTCs reveal a more intense increasing freezing intensity in terms of the annual sum of daily sub-zero temperatures from the riser to the ridge (2014/15) or tread center (2015/16), respectively (Table 1).

The vegetation maps (Figure 3e, f) show that about 75% of the lobe tread is covered by *D. octopetala*, in areas with high displacement rates such as the lower lobe tread (8–16.5 cm in 3 years) as well as in areas with nearly no displacement (<3 cm) such as the western lobe tread (Figure 3e). *D. octopetala* cover is absent at the sparsely vegetated ridge feature. Here, *Silene exscapa* occurs (>20 individuals, Figure 3e) and displacement rates are in an intermediate range (>3–8 cm in 3 years). *Salix hastata* occurs almost exclusively at the lobe risers (>15 individuals) with low displacement rates (<5 cm in 3 years). The occurrence of *Epilobium fleischeri* (>15 individuals) is limited to the very slowly moving western frontal lobe riser (<5 cm in 3 years), while this species is absent in the eastern part (Figure 3f) where higher displacement rates occur (3–16.5 cm in 3 years).

5 | DISCUSSION

5.1 | Applicability of UAV-based photogrammetry to map solifluction movement

Our UAV-based mapping approach provides surface solifluction movement rates with high spatial resolution, and the movement patterns derived are consistent with surface movement results from total station measurements. In comparison to previous approaches using tens of points,[13,16,18,40] we increased the spatial resolution of our assessment of solifluction lobe movement by about an order of magnitude (total 975 points). Due to the high spatial resolution, we could identify movement patterns of the whole landform, as well as detailed movement patterns at individual lobe elements. Differentiating movement according to landform elements is usually not possible with traditional methods such as tape measurements and total station surveys which rely on smaller numbers of markers arranged in a line in certain sections of the lobe (e.g., lobe center, upper and lower tread).[4,12] In addition to movement rates, UAV-based mapping also provides

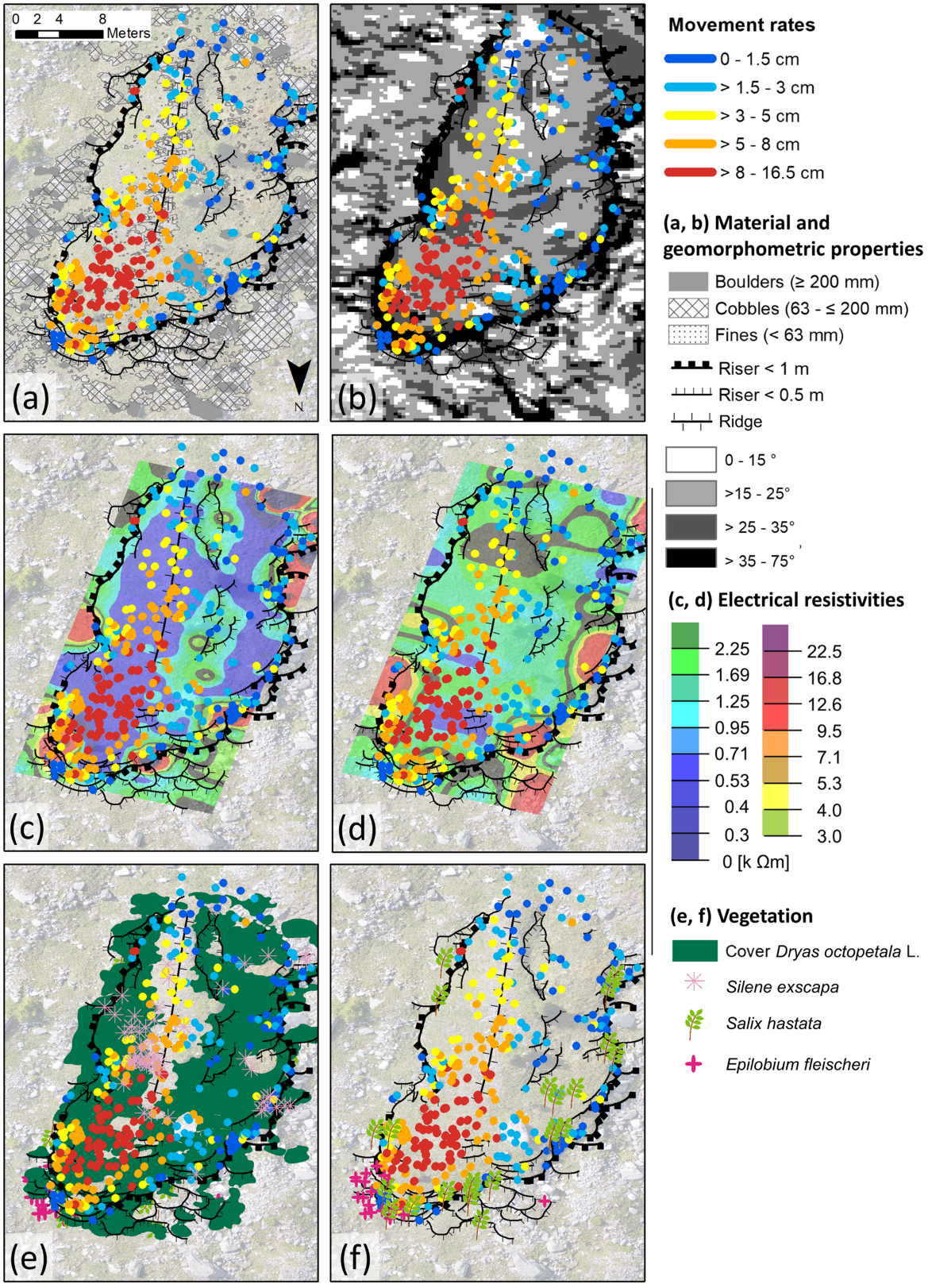

FIGURE 3 Geomorphometric, material and vegetation properties in relation to solifluction displacement (2014–2017) derived from unmanned aerial vehicle-based mapping. (a) Geomorphic map with landform elements and material properties in relation to displacement patterns. (b) Slope gradient map in relation to displacement patterns. Result from 3D ERT in relation to displacement patterns for (c) depth of 0–0.75 m and (d) depth of 0.75–1.5 m. Simplified vegetation map for (e) lobe tread and ridge feature as well as (f) lobe risers. See Eichel *et al.*[8] for more detailed vegetation maps [Colour figure can be viewed at wileyonlinelibrary.com]

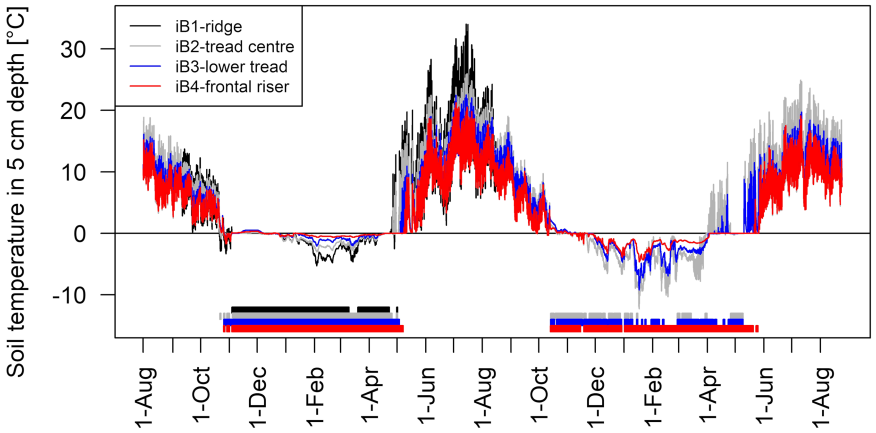

FIGURE 4 Soil temperatures at 5 cm depth recorded by iButton loggers 1–4 plotted versus time from August 2014 to occurrence. Note that data from iButton 1 are missing after August 17, 2015 [Colour figure can be viewed at wileyonlinelibrary.com]

TABLE 1 Thermal properties along the turf-banked solifluction lobe central axis from August 2014 to August 2016. Values for ground surface temperatures, snow cover and freeze–thaw activity are given for the periods 2014/2015 (left) and 2015/2016 (right)

Temperature logger	iButton 1 (iB1)	iButton 2 (iB2)	iButton 3 (iB3)	iButton 4 (iB4)
Location	Ridge	Tread center	Lower tread	Frontal riser
Species growing at logger locatio	*Trifolium pallescens*, *Salix serpyllifolia*	*Anthyllis vulneraria*, *Trifolium pallescens*	*Dryas octopetala*, *Poa alpina*	*D. octopetala*, *Salix reticulata*
Ground surface temperature (GST)				
MAGST [°C]	[a]/[b]	4.12/2.70	4.05/2.75	3.69/2.49
MWGST (DJF) [°C]	−1.61/[b]	−1.1/−4.41	−0.52/−3.19	−0.26/−1.98
MSGST (JJA) [°C]	[a]/[b]	12.58/11.9	12.09/10.0	11.09/9.92
Max. temperature [°C]	34.05/[b]	25.93/25.0	22.53/19.71	21.24/19.11
Annual sum of daily sub-zero temperatures [°C days]	233.5/[b]	157.1/536.9	87.7/373.9	46.3/228.4
Snow cover				
Duration of snow cover [days]	164/[b]	178/99	188/149	168/212
Freeze–thaw activity (at 5 cm depth)				
Number of freeze–thaw cycles (diurnal)	11(10)/[b]	4(3)/15(14)	2(1)/9(8)	2(1)/13(12)

[a]Incomplete data set.
[b]No data available due to loss of logger.

information on landform geomorphometry, such as slope gradient (Figure 3b), and ecological information, such as vegetation change (Figure 5a, b). This can be valuable in a biogeomorphic study linking vegetation and geomorphic dynamics.[41,42]

Both UAV-based mapping and traditional total station measurements show similar movement patterns (Figure 2a, b) with highest mean displacement rates (~2–2.4 cm yr^{-1}) observed at the lower eastern lobe tread. For total station measurements, measurement accuracy is below 1 cm, and only displacement at the lower eastern lobe with more than 2 cm yr^{-1} is considered significant (Figure 2b).

Our UAV-based mapping approach also has several limitations due to various sources of error. First, the average registration error (3.05 cm) is much higher than mean displacement rates per year at the TBL (1.55 cm) and higher than errors estimated for traditional tape measurements (1 cm)[16] and our total station measurements (<1 cm). Further potential errors lie in the measurement set-up and probably propagate through to the final products and derived displacement rates and patterns.[23,24] Different camera systems were used in 2014 and 2017, which required different camera calibrations in bundle adjustment.[24] Different light conditions in 2014 (cloudy) and 2017 (sunny) hampered identification of co-registration points, and subsequent feature tracking. To georeference the 2014 aerial imagery, GCPs measured with a differential GPS (accuracies of about 2–3 cm) were used. The use of GCPs can improve bundle adjustment, for example by improving camera calibration, but can also provide additional sources of error during photogrammetric processing in the range of measurement accuracies.[24] It is likely that some of the stable reference points used for co-registration moved between the measurements, as parent slopes are also affected by solifluction movement themselves.[20] Boulders used as reference points can move even faster than surrounding material by frost creep or as ploughing boulders.[43] However, we tried to exclude ploughing boulders by choosing only boulders as reference points without significant ploughing indicators such as any upslope furrows and downslope ridges.[43]

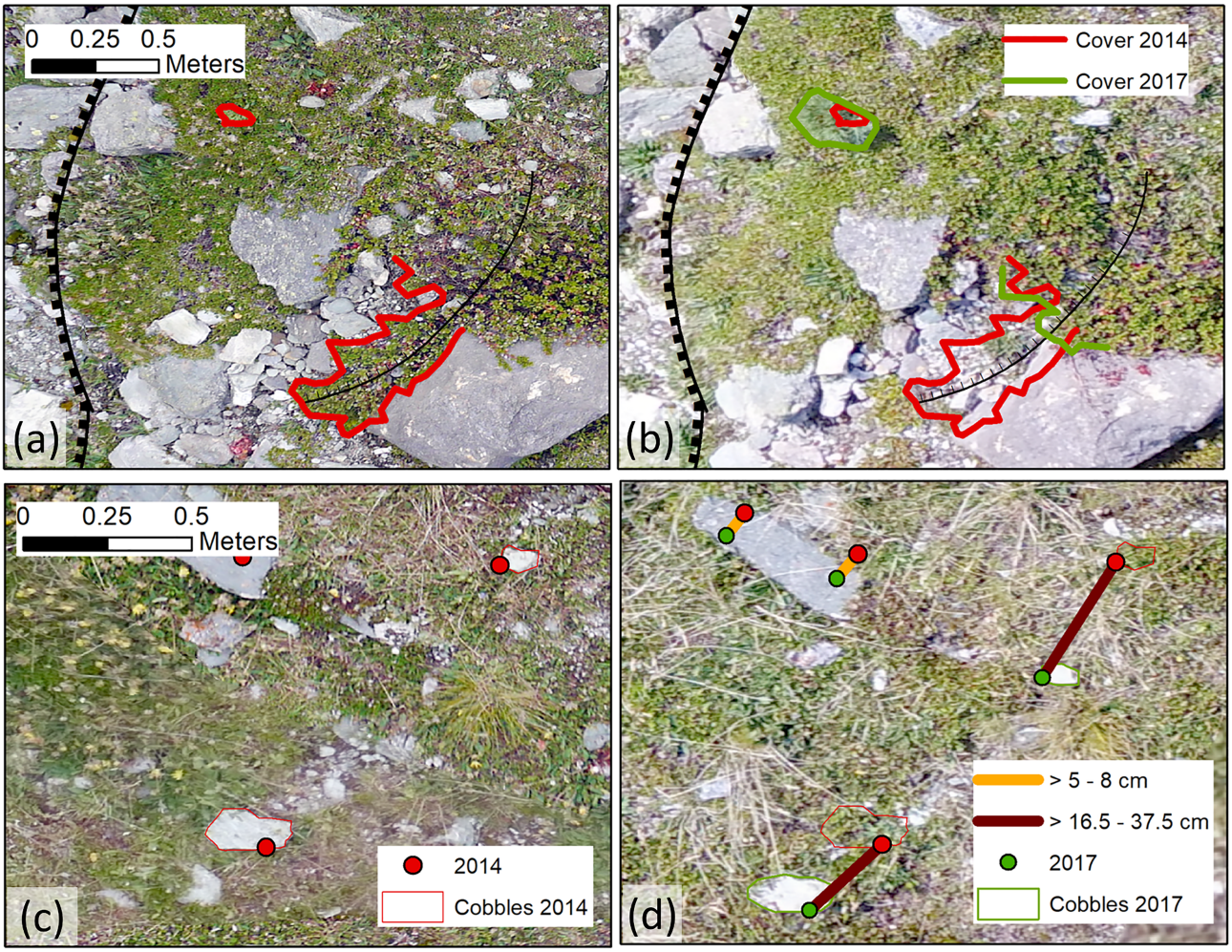

FIGURE 5 Vegetation change and displacement details extracted from unmanned aerial vehicle-based mapping. (a,b) Vegetation growth from 2014 to 2017. (c,d) Displacement of smaller rocks between 2014 and 2017 [Colour figure can be viewed at wileyonlinelibrary.com]

Potential movement of assumed stable points makes our movement results conservative and could affect derived movement patterns, especially when stable point movement is not uniform.

Thus, some of the observed displacement patterns could be explained by errors in the measurement set-up that propagated through photogrammetric processing. Previous studies observed radial distortion of digital elevation models (DEMs) created from UAV data[44] and deformations at the edges of photogrammetrically derived point clouds.[31] Radial distortions or point cloud deformations could explain displacement patterns at the parent slope, especially in the outer south-eastern and north-western edges (Figure 2a), although the use of GCPs for georeferencing the 2014 point cloud should have mitigated potential distortions.[44] An alternative explanation for the observed movement are turf-banked solifluction terraces found in these areas[45] which move quicker than the parent slope.[4,16] Finally, errors in our displacement rates will probably also arise from human disturbance as two ERT surveys have been carried out between the UAV flights during which material could have been moved. Overall, despite the limitations discussed, detected movement rates and patterns are consistent and in line with geomorphic knowledge of quicker movement of solifluction landforms than their parent slopes.

In contrast to most other studies,[31,46,47] we used a manual feature tracking approach on aerial imagery to determine solifluction movement. While a manual feature approach can be highly time-consuming in comparison with automatic feature tracking/image cross-correlation to determine surface displacement, this technique also has several advantages. For our data, automatic feature tracking was tested but not applicable mainly due to dense vegetation cover which limited feature selection. Using manual feature tracking, we were able to select the most suitable features for tracking, despite different light conditions, shadows, and vegetation cover and growth (cf. Figure 5a, b). Given more time for manual feature tracking, spatial resolution of solifluction movement can be easily improved and be focused on areas with conspicuous smaller scale movement patterns, such as the riser area (Figure 2c). Furthermore, manual feature tracking allowed us to systematically select "safe" features for tracking, such as rocks or stones firmly embedded in the soil. In contrast, tracking loose individual stones revealed unusually high displacement rates (16.5–37.5 cm in 3 years) that derive from surficial movement of individual rock samples which is not representative for movement of the solifluction lobe, or represent volumetrically insignificant movement by needle-ice creep (Figure 5c, d). These rates are excluded from the

analysis. Similar to automatic feature tracking, solifluction movement could not be assessed below dense vegetation cover due to the lack of trackable features. In a different setting, for example with less vegetation at a stone-banked lobe, or with improved feature selection, for example based on RGB-values to exclude vegetation, automatic feature tracking could be an alternative, less time-consuming approach.

5.2 | How to improve UAV-based mapping of solifluction movement

Generally, SfM photogrammetry can produce DEMs and orthophotos with small errors around 10–15 mm when distances between the UAV and the investigated object are sufficiently short (around 10 m).[24] Thus, UAV-based mapping is applicable to monitor annual solifluction movement in the range of millimeters to centimeters. To reach these high accuracies, a careful measurement set-up is required.[23,24] Georeferencing of UAV data by high-accuracy GCPs is the usual way to produce co-registered DEMs and orthophotos between two epochs.[24] However, the accuracy of this technique depends on measurement accuracy of the used differential GPS, which in our case was only 2–3 cm, and thus in the range of expected yearly solifluction rates.[18,40] In soil erosion studies, fixed stable GCPs were used to set up a local reference stable system for multi-temporal registration of the UAV data.[48] Eltner *et al*.[48] gave a reference net accuracy in the range of 1 mm in this set-up, which would be highly suitable for solifluction studies. Building a stable local reference system can be challenging at moving solifluction slopes. However, drilling GCP plates into bedrock or non-moving boulders or placing marking pipes at depths greater than solifluction movement depth could provide a suitable stable reference net. Additional GCPs installed in stable positions can serve as check points to evaluate the geometric accuracy of derived orthophotos and accuracy of co-registered orthophotos.[47] If large stable areas are available in the imagery, such as larger bedrock areas, an iterative closest points (ICP) or iterative closest proximity algorithm (ICProx) can be used to co-register two point clouds based on stable points or areas and produce an alignment between the two clouds as close as possible.[23,30,49]

Image processing and feature tracking, especially automatic feature tracking, can be improved by using the same UAV model and camera and conducting all flights with similar light conditions. To overcome problems with vegetation cover, additional surface markers which are excluded from GCPs could be introduced in areas with dense vegetation cover and tracked between the orthophotos, although this will lower the spatial resolution to values similar to traditional approaches.

Given a careful measurement set-up and rigorous photogrammetric processing,[23,24] we believe that UAV-based mapping can determine surface solifluction movement rates with at least the same accuracy as traditional methods, but with a much higher spatial resolution. By conducting repeated UAV flights over short periods, the temporal resolution of the technique could be strongly increased. For example, it could be possible to determine frost heave and creep processes at solifluction lobes based on DEMs of Difference.[27]

5.3 | Spatial patterns of solifluction movement and their relationship to material, geomorphometric, thermal and vegetation properties

Keeping the discussed uncertainties in mind, spatial patterns of surface movement of solifluction lobes from UAV-based mapping and total station measurements can be interpreted and related to material, geomorphometric, thermal and vegetation properties. Mean TBL movement rates from UAV-based mapping and total station measurements (1.55/0.83 cm yr^{-1}) are lower than movement rates reported for similar Alpine settings such as the Austrian Alps (3.5–6.8 cm yr^{-1})[40] or Niwot Ridge, Colorado (0.3–4.3 cm yr^{-1}).[4] These differences in mean TBL movement rates could be attributed to different climatic conditions and site-specific controls,[16,40] such as material properties or slope gradient, or to the fact that solifluction movement is often measured only at the lobe center or lower lobe tread,[12,50] which are often the most quickly moving lobe parts.[4,51,52] In this study, displacement rates of the lower tread range from 1.9–2.4 cm yr^{-1} from UAV-based mapping to 2.18 cm yr^{-1} from total station measurements and are, therefore, in a similar range as previously reported. Our results show that overall displacement rates are spatially highly variable (from 0.27 to 16.29 cm in 3 years) with distinct spatial patterns. The central lobe axis moves quicker than its sides, with fastest movement observed at the lower lobe tread (Figure 2a, b), in agreement with studies on alpine and arctic solifluction lobes.[4,51,52] The large range of internal movement rates indicates that mean rates derived from point measurements could severely over- or underestimate local solifluction movement, depending on point locations.

Detected spatial movement patterns relate to the lobe element risers, tread and ridge and can potentially be explained by investigated material, geomorphometric, thermal and vegetation properties. Slower displacement at the lobe risers (mean 0.63 cm yr^{-1}) than at the lobe tread (mean 1.57 cm yr^{-1}) is typical for solifluction lobes[4,53] and is probably related to material properties of the lobe. ERT results (Figure 3c, d) show that areas with highest resistivities (>7.1 kΩm) occur at the lobe risers at depths of 0–1.5 m. High resistivities indicate the occurrence of coarse material,[7] which is also visible in the geomorphic map (Figure 3a). Cobble and boulder concentrations at lobe risers are typical for solifluction lobes[54-56] and enable water seepage,[7] which inhibits ice segregation and thereby solifluction processes. The species composition at the lobe risers supports low movement rates. Several of the species have low tensile strength or fragile roots and rhizomes (*E. fleischeri*, *S. hastata*) and require relatively stable conditions.[57-60] Smaller scale displacement patterns at the eastern lobe front (Figure 2a, b) and the western lateral riser (Figure 2d) suggest different mechanisms of frontal and lateral advance of the lobe. At the eastern lobe front, displacement of multiple surficial layers with higher rates (mean 1.26 cm yr^{-1}) could explain the multistep lobe front made up by several smaller risers (< 0.5 m; Figure 3a).[50] At the

western lateral riser, opposing displacement of the upper and lower riser areas (Figure 2d) could indicate caterpillar-like displacement, resulting from decreasing displacement with increasing soil depth[4,50] where "rolling" of the upper soil layers also potentially moves the rocks below towards the lobe.

At the lobe tread, the observed amplified displacement along the central and lower part (mean 1.9 cm, 1.96 cm yr^{-1}) can be explained jointly by material, geomorphometric, thermal and vegetation properties (Figures 2–4). ERT results show lowest near-surface (0–0.75 m) resistivities (<0.71 kΩm) at the tread (Figure 3a), which we interpret as fine material that enables higher moisture contents.[7] Higher soil moisture along the lobe tread can furthermore be promoted by water channelization due to the coarse and dry risers[20] and water drainage downslope,[61] especially in the slightly steeper inclined lower lobe tread (Figure 3b). Besides soil moisture, soil temperatures below the freezing point are another precondition for solifluction. Temperature data show a decreasing cooling trend along the lobe tread towards the frontal riser (Figure 4, Table 1), with amplified ground cooling in 2015/2016 probably due to spurious gaps in snow cover.[61,62] Pronounced winter cooling especially at the central tread, indicated by lower MWGST and high annual sum of daily sub-zero temperatures, enhances frost penetration and generation of ice lenses at greater depths, and therefore it potentially enables deeper solifluction movement. At the lower tread, comparatively lower freezing rates under longer snow cover amplify ice segregation[63] and thereby shallow frost creep and gelifluction. Similar to snow cover, vegetation properties also affect freezing rates. Most of the lobe tread is covered by the ecosystem engineer *D. octopetala* (Figure 3c), which possesses a thick organic mat that probably decreases frost penetration, but promotes temperatures favoring ice segregation during annual FTCs.[64] In addition, *D. octopetala* roots can increase soil shear strength at the surface and pore water pressures at greater depth through enhanced infiltration.[8,65,66] By enhancing ice segregation and pore water pressures, ecosystem engineering by *D. octopetala* could promote annual frost creep and deep gelifluction[8] at the tread with a convexo-concave movement.[1,5]

Lower displacement rates at the lobe ridge (1.2 cm yr^{-1}) in comparison to other tread areas could result from differing geomorphometric, thermal and vegetation properties. While low resistivities (<0.71 kΩm) indicate material conditions similar to the tread,[7] the ridge is slightly less inclined, snow cover is several days shorter in 2014/2015 (Figure 4, Table 1) and vegetation cover is low (Figure 3e). Shorter snow duration and low vegetation cover can explain increased diurnal freeze–thaw activity in late October and early November 2014 (Figure 4, Table 1) and promote, together with frost-susceptible fines (Figure 3a), needle ice and diurnal frost creep.[1] The efficiency of freezing at the ridge is supported by the occurrence of the frost-disturbance indicator species *S. exscapa* (Figure 3e).[67] Irregular rock movement observed at the lower part of the ridge (Figure 2c) could have been caused by overturning of clasts by needle ice and frost creep.[27,68] However, small-scale movement patterns could also result from human disturbance during the ERT surveys carried out between 2014 and 2017.

6 | CONCLUSION

We used a novel UAV-based SfM photogrammetry approach to map solifluction movement at a TBL in Turtmann glacier foreland, Switzerland. Our results show that:

1. UAV-based SfM photogrammetry is a suitable tool to map solifluction movement a high spatial resolution (one point per m^2, total > 900 points). Detected displacement rates (mean 1.55 cm yr^{-1}) and patterns are in accordance with results from a traditional total station survey (mean 0.83 cm yr^{-1}). However, a careful measurement set-up and rigorous photogrammetric processing are required to produce reliable results for short-term (annual and shorter) movement rates.
2. TBL movement varies between lobe tread, risers and a ridge feature, and can be interpreted with the help of material, geomorphometric, thermal and vegetation properties. Highest and significant movement (1.9–2.4 cm yr^{-1}) occurred at the lower lobe tread, where fine material, highest moisture contents and dense ecosystem engineer cover probably promote annual frost creep and gelifluction. High risers build up due to slower movement of dry and coarse riser material (mean 0.63 cm yr^{-1}), movement mechanisms potentially differ between the frontal and lateral risers. At a fine material-rich ridge feature, shorter snow cover duration, low vegetation cover and a resulting higher freeze–thaw activity could promote diurnal needle ice and frost creep with intermediate movement rates (mean 1.2 cm yr^{-1}) and irregular movement patterns.

Our study demonstrates that solifluction movement rates can be highly variable within one landform due to heterogeneous material, geomorphometric, thermal and vegetation properties. Thus, solifluction movement needs to be assessed at high spatial resolution, which can be provided by UAV-based SfM photogrammetry. The combination of UAV-based mapping of solifluction movement, assessment of spatial movement controls and classic approaches to assess subsurface movement[12,13,52] has good potential to improve our understanding of solifluction processes and landform development and can benefit future studies.

ACKNOWLEDGEMENTS

This study is part of the BIMODAL (Biogeomorphic dynamics on lateral moraines in the Turtmann glacier foreland, Switzerland) project, funded by the German Research Foundation DFG (DI 414/22-1). J. Eichel acknowledges additional support by the Dr Hohmann award of the Gesellschaft für Erdkunde zu Köln e.V. and the Humboldt-Ritter-Penck-Stiftung of the Gesellschaft für Erdkunde zu Berlin. Vehicle access to the Turtmann glacier foreland was kindly granted by GOUGRA AG. The authors thank Uwe Weidner (Institute of Photogrammetry and Remote Sensing, KIT) for initial tests on automatic feature tracking on the lobe data. Fieldwork assistance by Karoline Messenzehl, Andreas Ewald, Katharina Eibisch, Nele Meyer, Katrin Hoffmann, Nikola Schulte-

Kellinghaus, Sebastian Unger and Marion Neumann is highly appreciated. The authors thank the three reviewers for their valuable comments that helped to improve the manuscript.

ORCID

Jana Eichel https://orcid.org/0000-0001-6116-084X
Daniel Draebing https://orcid.org/0000-0001-6379-4707

REFERENCES

1. Matsuoka N. Solifluction rates, processes and landforms: a global review. *Earth Sci Rev*. 2001;55(1):107-134. https://doi.org/10.1016/S0012-8252(01)00057-5
2. Berthling I, Etzelmüller B, Larsen CK, Nordahl K. Sediment fluxes from creep processes at Jomfrunut, southern Norway. *Norsk Geograf Tidsskriftâ-Norwegian J Geogr*. 2002;56(2):67-73. https://doi.org/10.1080/002919502760056378
3. Draebing D, Eichel J. Divergence, convergence and path-dependency of paraglacial adjustment of Alpine lateral moraine slopes. *Land Degradation Dev*. 2018;29(6):1979-1990. https://doi.org/10.1002/ldr.2983
4. Benedict JB. Downslope soil movement in a Colorado Alpine region: rates, processes, and climatic significance. *Arctic Alpine Res*. 1970;2(3):165-226. https://doi.org/10.2307/1550306
5. Harris C, Smith JS, Davies MCR, Rea B. An investigation of periglacial slope stability in relation to soil properties based on physical modelling in the geotechnical centrifuge. *Geomorphology*. 2008;93(3–4):437-459. https://doi.org/10.1016/j.geomorph.2007.03.009
6. Kinnard C, Lewkowicz AG. Frontal advance of turf-banked solifluction lobes, Kluane range, Yukon territory, Canada. *Geomorphology*. 2006;73(3):261-276. https://doi.org/10.1016/j.geomorph.2005.06.010
7. Draebing D, Eichel J. Spatial controls of turf-banked solifluction lobes and their role for paraglacial adjustment in glacier forelands. *Permafrost Periglac Process*. 2017;28(2):446-459. https://doi.org/10.1002/ppp.1930
8. Eichel J, Draebing D, Klingbeil L, et al. Solifluction meets vegetation: the role of biogeomorphic feedbacks for turf-banked solifluction lobe development. *Earth Surf Process Landf*. 2017;42(11):1623-1635. https://doi.org/10.1002/esp.4102
9. Eichel J, Corenblit D, Dikau R. Conditions for feedbacks between geomorphic and vegetation dynamics on lateral moraine slopes: a biogeomorphic feedback window. *Earth Surf Process Landf*. 2016;41(3):406-419. https://doi.org/10.1002/esp.3859
10. Smith J. Some moving soils in Spitsbergen. *J Soil Sci*. 1956;7(1):11-21. https://doi.org/10.1111/j.1365-2389.1956.tb00857.x
11. Kinnard C, Lewkowicz AG. Movement, moisture and thermal conditions at a turf-banked solifluction lobe, Kluane range, Yukon territory, Canada. *Permafrost Periglac Process*. 2005;16:1-15.
12. Matsuoka N. Solifluction and mudflow on a limestone periglacial slope in the Swiss Alps: 14 years of monitoring. *Permafrost Periglac Process*. 2010;21(3):219-240. https://doi.org/10.1002/ppp.678
13. Jaesche P, Veit H, Huwe B. Snow cover and soil moisture controls on solifluction in an area of seasonal frost, eastern Alps. *Permafrost Periglac Process*. 2003;14(4):399-410. https://doi.org/10.1002/ppp.471
14. Price LW. The developmental cycle of Solifluction lobes. *Annals Assoc Am Geogr*. 1974;64(3):430-438. https://doi.org/10.1111/j.1467-8306.1974.tb00991.x
15. Rapp A. Recent development of mountain slopes in Kärkevagge and surroundings, northern Scandinavia. *Geogr Ann*. 1960;42(2/3):65-200. https://doi.org/10.2307/520126
16. Ridefelt H, Boelhouwers J, Etzelmüller B. Local variations of solifluction activity and environment in the Abisko Mountains, northern Sweden. *Earth Surf Process Landf*. 2011;36(15):2042-2053. https://doi.org/10.1002/esp.2225
17. Jaesche P, Huwe B, Stingl H, Veith H. Temporal variability of alpine solifluction: a modelling approach. *Geograph Helv*. 2002;57:157-169. https://doi.org/10.5169/seals-71294
18. Gamper M. *Heutige Solifluktionsbeträge von Erdströmen und klimamorphologische Interpretation fossiler Böden*. Lüdin AG: Liestal; 1981 https://www.parcs.ch/snp/pdf_public/1601_gamper_solifluktion_nf_1981.pdf.
19. Matsuoka N. Combining time-lapse photography and multisensor monitoring to understand frost creep dynamics in the Japanese Alps. *Permafrost Periglac Process*. 2014;25(2):94-106. https://doi.org/10.1002/ppp.1806
20. Benedict JB. Frost creep and gelifluction features: a review. *Quatern Res*. 1976;6(1):55-76. https://doi.org/10.1016/0033-5894(76)90040-5
21. Eckerstorfer M, Eriksen HØ, Rouyet L, Christiansen HH, Lauknes TR, Blikra LH. Comparison of geomorphological field mapping and 2D-InSAR mapping of periglacial landscape activity at Nordnesfjellet, northern Norway. *Earth Surf Process Landf*. 2018;43(10):2147-2156. https://doi.org/10.1002/esp.4380
22. Eckerstorfer M, Malnes E, Christiansen HH. Freeze/thaw conditions at periglacial landforms in Kapp Linné, Svalbard, investigated using field observations, in situ, and radar satellite monitoring. *Geomorphology*. 2017;293:433-447. https://doi.org/10.1016/j.geomorph.2017.02.010
23. Micheletti N, Chandler JH, Lane SN. Structure from motion (SFM) photogrammetry. In: Clark LE, Nield JM, eds. *Geomorphological Techniques*. Online ed.), Chap. 2, Sec. 2.2 London: British Society for Geomorphology; 2015.
24. Smith MW, Carrivick JL, Quincey DJ. Structure from motion photogrammetry in physical geography. *Progr Phys Geogr Earth Environ*. 2016;40(2):247-275. https://doi.org/10.1177/0309133315615805
25. Westoby MJ, Brasington J, Glasser NF, Hambrey MJ, Reynolds JM. 'Structure-from-motion' photogrammetry: a low-cost, effective tool for geoscience applications. *Geomorphology*. 2012;179:300-314. https://doi.org/10.1016/j.geomorph.2012.08.021
26. Dąbski M, Zmarz A, Pabjanek P, Korczak-Abshire M, Karsznia I, Chwedorzewska KJ. UAV-based detection and spatial analyses of periglacial landforms on Demay point (King George Island, South Shetland Islands, Antarctica). *Geomorphology*. 2017;290:29-38. https://doi.org/10.1016/j.geomorph.2017.03.033
27. Ponti S, Cannone N, Guglielmin M. Needle ice formation, induced frost heave, and frost creep: a case study through photogrammetry at Stelvio pass (Italian Central Alps). *Catena*. 2018;164:62-70. https://doi.org/10.1016/j.catena.2018.01.009
28. Dall'Asta E, Forlani G, Roncella R, Santise M, Diotri F, Morra di Cella U. Unmanned aerial systems and DSM matching for rock glacier monitoring. *ISPRS J Photogram Remote Sens*. 2017;127:102-114. https://doi.org/10.1016/j.isprsjprs.2016.10.003
29. Piermattei L, Carturan L, de Blasi F, et al. Suitability of ground-based SfM–MVS for monitoring glacial and periglacial processes. *Earth Surf Dyn*. 2016;4(2):425-443. https://doi.org/10.5194/esurf-4-425-2016
30. Vivero S, Lambiel C. Monitoring the crisis of a rock glacier with repeated UAV surveys. *Geograph Helv*. 2019;74(1):59-69. https://doi.org/10.5194/gh-74-59-2019
31. Kääb A, Girod L, Berthling I. Surface kinematics of periglacial sorted circles using structure-from-motion technology. *The Cryosphere*. 2014;8(3):1041-1056. https://doi.org/10.5194/tc-8-1041-2014
32. Bearth P. *Geologischer Atlas Der Schweiz. Blatt 1308 St. Niklaus, Erläuterungen*. Bern: Kümmerly & Frey; 1980.
33. Labhart TP. *Geologie Der Schweiz*. Bern: Ott-Verlag; 2009.
34. MeteoSwiss. Climate Data Station Turtmann, 2013-2017. 2017.
35. Nyenhuis M, Hölzle M, Dikau R. Rock glacier mapping and permafrost distribution modelling in the Turtmanntal, Valais, Switzerland. *Z Geomorphol*. 2005;49(3):275-292.

36. Whitehead K, Moorman BJ, Hugenholtz CH. Brief communication: low-cost, on-demand aerial photogrammetry for glaciological measurement. *The Cryosphere*. 2013;7(6):1879-1884. https://doi.org/10.5194/tc-7-1879-2013
37. Heunecke O, Kuhlmann H, Welsch W, et al. *Handbuch Ingenieurgeodäsie: Auswertung geodätischer Überwachungsmessungen*2, neu bearb.u.erw. Auflage. Berlin: Wichmann; 2013.
38. Keller M, Hungerbuehler G, Knecht O, et al. iAssist: Rapid deployment and maintenance of tiny sensing systems. *Proceedings of the 8th ACM Conference on Embedded Networked Sensor Systems*. 2010:401–402.
39. Schmid M-O, Gubler S, Fiddes J, Gruber S. Inferring snowpack ripening and melt-out from distributed measurements of near-surface ground temperatures. *The Cryosphere*. 2012;6(5):1127-1139. https://doi.org/10.5194/tc-6-1127-2012
40. Kellerer-Pirklbauer A. Solifluction rates and environmental controls at local and regional scales in Central Austria. *Norsk Geograf Tidsskriftâ Norwegian J Geogr*. 2017;72:37-56. https://doi.org/10.1080/00291951.2017.1399164
41. Hortobágyi B, Corenblit D, Vautier F, et al. A multi-scale approach of fluvial biogeomorphic dynamics using photogrammetry. *J Environ Manage*. 2016;202:348-362. https://doi.org/10.1016/j.jenvman.2016.08.069
42. Vautier F, Corenblit D, Hortobágyi B, Fafournoux L, Steiger J. Monitoring and reconstructing past biogeomorphic succession within fluvial corridors using stereophotogrammetry. *Earth Surf Process Landf*. 2016;41(10):1448-1463. https://doi.org/10.1002/esp.3962
43. Ballantyne CK. Measurement and theory of ploughing boulder movement. *Permafrost Periglac Process*. 2001;12(3):267-288. https://doi.org/10.1002/ppp.389
44. James MR, Robson S. Mitigating systematic error in topographic models derived from UAV and ground-based image networks. *Earth Surf Process Landf*. 2014;39(10):1413-1420. https://doi.org/10.1002/esp.3609
45. Eichel J, Draebing D, Meyer N. From active to stable: Paraglacial transition of Alpine lateral moraine slopes. *Land Degrad Dev*. 2018;29(11):4158-4172. https://doi.org/10.1002/ldr.3140
46. Peppa MV, Mills JP, Moore P, Miller PE, Chambers JE. Brief communication: Landslide motion from cross correlation of UAV-derived morphological attributes. *Nat Hazards Earth Syst Sci*. 2017;17(12):2143-2150. https://doi.org/10.5194/nhess-17-2143-2017
47. Lucieer A, de Jong SM, Turner D. Mapping landslide displacements using structure from motion (SfM) and image correlation of multitemporal UAV photography. *Progr Phys Geogr Earth Environ*. 2014;38(1):97-116. https://doi.org/10.1177/0309133313515293
48. Eltner A, Baumgart P, Maas H-G, Faust D. Multi-temporal UAV data for automatic measurement of rill and interrill erosion on loess soil. *Earth Surf Process Landf*. 2015;40(6):741-755.
49. Wujanz D, Avian M, Krueger D, Neitzel F. Identification of stable areas in unreferenced laser scans for automated geomorphometric monitoring. *Earth Surf Dyn*. 2018;6(2):303-317. https://doi.org/10.5194/esurf-6-303-2018
50. Ballantyne CK. A 35-year record of Solifluction in a maritime periglacial environment. *Permafrost Periglac Process*. 2013;24(1):56-66. https://doi.org/10.1002/ppp.1761
51. Zuber E. *Pflanzensoziologische und ökologische Untersuchungen an Strukturrasen (besonders Girlandenrasen) im schweizerischen Nationalpark*. 60 Lüdin: Liestal; 1968 https://www.parcs.ch/snp/pdf_public/1563_zuber_strukturrasen_nf_1968.pdf.
52. Harris C, Kern-Luetschg M, Smith F, Isaksen K. Solifluction processes in an area of seasonal ground freezing, Dovrefjell, Norway. *Permafr Periglac Process*. 2008;19(1):31-47. https://doi.org/10.1002/ppp.609
53. Gengnian L, Heigang X, Zhijiu C. Gelifluction in the alpine periglacial environment of the Tianshan Mountains, China. *Permafr Periglac Process*. 1995;6(3):265-271. https://doi.org/10.1002/ppp.3430060308
54. Williams PJ. Some investigations into solifluction features in Norway. *Geogr J*. 1957;123(1):42-55. https://doi.org/10.2307/1790722
55. Matthews JA, Harris C, Ballantyne CK. Studies on a gelifluction lobe, Jotunheimen, Norway: ^{14}C chronology, stratigraphy, sedimentology and palaeoenvironment. *Geogr Ann Ser B*. 1986;68(4):345-360. https://doi.org/10.2307/521526
56. Harris C. Engineering properties, groundwater conditions, and the nature of soil movement on a solifluction slope in North Norway. *Q J Eng Geol Hydrogeol*. 1977;10:27-43. https://doi.org/10.1144/gsl.qjeg.1977.010.01.02
57. Jonasson S. Influence of frost heaving on soil chemistry and on the distribution of plant growth forms. *Geogr Ann Ser B*. 1986;68(3):185-195. https://doi.org/10.2307/521458
58. Ellenberg H. *Vegetation Ecology of Central Europe*. 4th ed. Cambridge, UK: Cambridge University Press; 2009.
59. Pohl M, Graf F, Buttler A, Rixen C. The relationship between plant species richness and soil aggregate stability can depend on disturbance. *Plant Soil*. 2012;355(1–2):87-102. https://doi.org/10.1007/s11104-011-1083-5
60. Hudek C, Sturrock CJ, Atkinson BS, Stanchi S, Freppaz M. Root morphology and biomechanical characteristics of high altitude alpine plant species and their potential application in soil stabilization. *Ecol Eng*. 2017;109:228-239. https://doi.org/10.1016/j.ecoleng.2017.05.048
61. Luetschg M, Lehning M, Haeberli W. A sensitivity study of factors influencing warm/thin permafrost in the Swiss Alps. *J Glaciol*. 2008;54(187):696-704. https://doi.org/10.3189/002214308786570881
62. Luetschg M, Haeberli W. Permafrost evolution in the Swiss Alps in a changing climate and the role of the snow cover. *Norsk Geograf Tidsskriftâ-Norwegian J Geogr*. 2005;59(2):78-83. https://doi.org/10.1080/00291950510020583
63. Matsuoka N, Murton J. Frost weathering: recent advances and future directions. *Permafrost Periglac Process*. 2008;19(2):195-210. https://doi.org/10.1002/ppp.620
64. Williams PJ, Smith MW. *The Frozen Earth: Fundamentals of Geocryology*. Cambridge, UK: Cambridge University Press; 1989.
65. Ghestem M, Sidle RC, Stokes A. The influence of plant root systems on subsurface flow: implications for slope stability. *Bioscience*. 2011;61(11):869-879. https://doi.org/10.1525/bio.2011.61.11.6
66. Eibisch K, Eichel J, Dikau R. Root tensile strength assessment of Dryas octopetala L. and implications for its engineering mechanism on lateral moraine slopes (Turtmann Valley, Switzerland). *Geophys Res Abstracts*. 2015:EGU2015–5146.
67. Körner C. *Alpine Plant Life: Functional Plant Ecology of High Mountain Ecosystems*. Berlin, Germany: Springer; 2003.
68. Li A, Matsuoka N, Niu F. Frost sorting on slopes by needle ice: a laboratory simulation on the effect of slope gradient. *Earth Surf Process Landf*. 2018;43(3):685-694. https://doi.org/10.1002/esp.4276

SUPPORTING INFORMATION

Additional supporting information may be found online in the Supporting Information section at the end of this article.

How to cite this article: Eichel J, Draebing D, Kattenborn T, et al. Unmanned aerial vehicle-based mapping of turf-banked solifluction lobe movement and its relation to material, geomorphometric, thermal and vegetation properties. *Permafrost and Periglac Process*. 2020;31:97–109. https://doi.org/10.1002/ppp.2036